A Finite Element Shell Analysis of Guard Cell Deformations

J. Robert Cooke, Josse G. De Baerdemaeker, Richard H. Rand, Herbert A Mang
ASSOC. MEMBER ASAE — ASSOC. MEMBER ASAE

ABSTRACT

IN this paper the width of the stomatal aperture, as postulated by von Mohl in 1856, is shown to be a function of the hydrostatic (turgor) pressure in the guard cells, P_g, and the pressure, P_s, of the immediately surrounding epidermal cells, which will be referred to as the subsidiary cells in this paper. The aperture does not depend solely upon the pressure difference (P_g-P_s) as believed by Ursprung and Blum (1924) and Stålfelt (1966). Instead, aperture width is shown to be a simple multilinear relationship (i.e., a linear combination) of P_g and P_s. The recent research by Glinka (1971) and Edwards, Meidner and Sheriff (1976), showing the relative contributions of the opposing pressures P_g and P_s, is, thus, given a simple and lucid interpretation.

The analysis of a guard cell as an elliptical torus shows that a stomate *could* function without either of the two conditions classically believed to be essential (Meyer et al. 1960, p. 84, Meidner and Mansfield 1968, pp. 14-17, Bidwell 1974, p. 298). The "thickened wall" (ventral wall) of the guard cell facing the aperture need not necessarily be stiffer than the dorsal wall common to the adjacent epidermal cell for the proper functioning of a stomate. The radially oriented cellulose microfibrils in the guard cell wall are not vital but are important for quite different reasons than claimed by Aylor et al. (1973). Consideration of the radial stiffening by means of the introduction of a mechanically equivalent orthogonally anisotropic (i.e., orthotropic) material causes the aperture width to be more sensitive to a unit increment in P_s than to a unit increment in P_g (for parameters of physical interest). The guard cell volume, however, is smaller than the adjacent cell volume and P_g is believed to be larger than P_s, in general. We conjecture that this increased sensitivity for the subsidiary cell (i.e., closing) pressure is important for the functioning of the feedback control loops regulating the aperture width. We define an *antagonism ratio* to characterize this property. The pore length in the model is shown to be surprisingly constant during opening, as is reported for many species (Meidner and Mansfield 1968, p. 12).

The guard cell is generally believed to bulge into the neighboring epidermal cell upon opening (Meidner and Mansfield 1968, p. 15). However, the shell model suggests that the outermost portion of the guard cell at the widest point (and not visible in an *in vivo* situation) actually moves away from the neighboring cell. The approximate point at which the exposed surface of the epidermal cell joins the guard cell exhibits only limited motion. Note that there are especially thin regions here in the epidermal cell thought to behave as hinges (Hautgelenke). Even when the extreme, unphysiological case of a fixed aperture length is imposed, the outermost perimeter moves away from the adjacent cell. If the epidermis is opaque, the view from *outside* the leaf suggests that the guard cell "bulges" into the neighboring cell, as claimed in the classical hypothesis, provided the stiffening effect of the micellae is sufficiently prominent and provided the guard cell pressure is significantly larger than the epidermal cell pressure.

The opposing influence of the turgor pressure in the guard cells and in the adjacent epidermal cells is shown to be an inherent part of the stomatal mechanism (von Mohl 1856). Pressure influence coefficients for the guard cell are defined and related to parameter changes, e. g., material and thickness.

The multilinear relationship of aperture width to the opposing turgor pressures was found and revealed that pore width does not depend solely on the pressure difference between the guard cell and the adjacent epidermal cell. Finally, the theory developed is shown to embrace and to clarify the experimental results of Glinka's plasmolytic study (1971) and the direct method of Edwards et al. (1976).

Article was submitted for publication in June 1976; reviewed and approved for publication by the Soil and Water Division of ASAE in October 1976. This paper was presented as ASAE Paper 76-5526.

The authors are: J. ROBERT COOKE, Associate Professor, Agricultural Engineering Dept., Cornell University, Ithaca, NY; JOSSE G. De BAERDEMAEKER, Aangesteld Navorser, NFWO, Katholieke Universiteit Leuven, Belgium,; RICHARD H. RAND, Associate Professor, Theoretical and Applied Mechanics Dept., and HERBERT A. MANG, Visiting Fellow, Structural Engineering Dept., Cornell University, Ithaca, NY.

Acknowledgment: The authors gratefully acknowledge the valuable discussions with T. Sinclair and M. Delwiche and the technical assistance of D. Chapman, D. Moutner, R. Stroshine, R. Krizek and H. Levinson. The authors are grateful to R. H. Gallagher for permission to use the finite element shell analysis computer program (FESIA) developed in the Dept. of Structural Engineering at Cornell University. The authors thank M. Kaplan for introducing them to the techniques of computer graphics.

INTRODUCTION

Photosynthesis and transpiration are, to a large extent, controlled by stomata, the tiny, variable aperture pores on the surface of higher land plants; these stomata are especially prevalent on leaves. Virtually all of the carbon assimilated by higher land plants during the photosynthetic process enters the plant through the stomata. Furthermore, most of the water reaching the ground as precipitation, or supplied by irrigation, passes out of the plant through these pores. Thus a stomatal configuration most favorable for entry of carbon dioxide into the plant is simultaneously unfavorable for the water status of the plant. The role of stomates in mediating the balance between photosynthesis and transpiration is profoundly important in crop production and has continued as an active, vital area of research for more than 125 years.

There are two principal types of stomates — the long, narrow graminaceous type found in grasses (e. g.

This article is reprinted from the TRANSACTIONS of the ASAE (Vol. 19, No. 6, pp. 1107, 1108, 1109, 1110, 1111, 1112, 1113, 1114, 1115, 1116, 1117, 1118, 1119, 1120, 1121, 1976
Published by the American Society of Agricultural Engineers, St. Joseph, Michigan

FIG. 1 Scanning electron microscope view by Troughton and Donaldson of stomata on lower surface of a cucumber leaf [reproduced by permission of John Troughton].

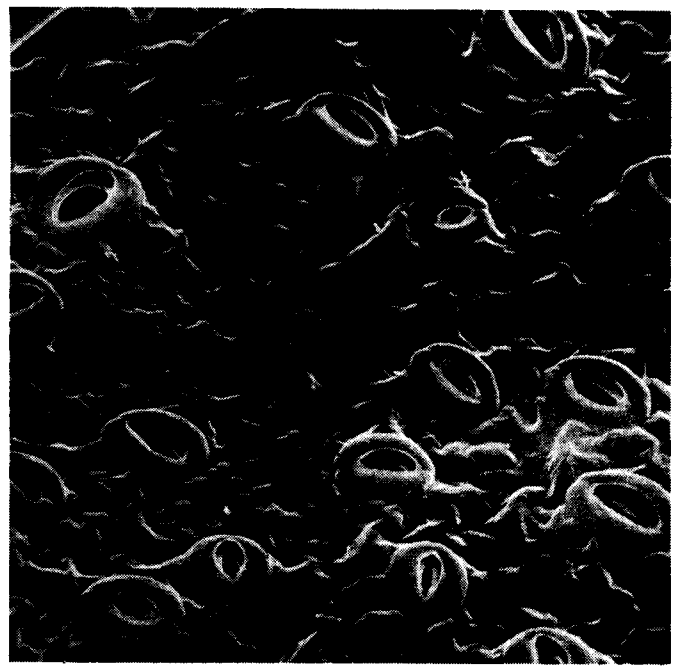

FIG. 2 Closeup view of cucumber stomate by Troughton and Donaldson [reproduced by permission of John Troughton].

corn) and the elliptical or kidney-shaped type typical, for example, of beans. We will present an analysis of the mechanical deformations of this latter class and will describe the response of the guard cells (which form the pore) to changes in both internal pressure of the guard cells and in the specialized epidermal cells surrounding the guard cells. We will also critically examine the classical hypotheses of the mechanism of guard cell movement.

Recently, classical beam theory analyses of guard cell deformations have been attempted to validate the classical hypotheses concerning stomatal opening. However, the advent of a significantly more powerful and sophisticated tool of analysis for the study of doubly curved, doubly connected shells such as the guard cells — the finite element method — and the availability of large, general-purpose digital computers, have made possible a more realistic treatment of the guard cell problem.

LITERATURE REVIEW

The literature on stomata is voluminous. In addition to the papers already mentioned, the following general reviews are particularly useful here: Heath 1959a,b, Kramer 1959, von Guttenberg 1959, Esau 1965. Slatyer 1967, Meidner and Mansfield 1968, Raschke 1975. There is great variety in the geometrical and physical characteristics of stomates, such as size, shape, and surface density. Meidner and Mansfield (1968) have tabulated data on numerous species. For example, the widely studied *Vicia faba* has approximately 65 and 75 stomates per mm^2 on the lower and upper leaf surfaces, respectively. The overall stomatal apparatus viewed from outside the leaf is approximately 40 x 30 microns when open and 40 x 23 microns when closed. The guard cell dimensions (exclusive of the aperture) are approximately 40 x 9 microns when open and 40 x 11 microns closed. The pore length stays constant at 25 microns and the pore width changes from approximately 1 to 12 microns. The enclosed volume of a pair of guard cells is on the order of 10^{-11} liters (Raschke 1975). In the present study we shall abstract a "generic" stomate, rather than concentrate on the details of any particular species.

Fig. 1 shows a scanning electron microscope view of the stomates on the lower surface of a cucumber leaf (Troughton and Donaldson 1972). Fig. 2, taken from the same publication, shows greater detail for a fully open pair of guard cells.

The gradient in water potential, of which hydrostatic pressure is one component, governs the movement of water into the guard and epidermal cells. Heath (1959a) presents photographs which indicate that the release of guard cell turgor pressure causes aperture closure while the release of the pressure in the adjacent epidermal cell causes further opening. In this study we shall be concerned only with stomatal opening in relation to the hydrostatic pressure of the cells and not with the physical or biochemical considerations governing the movement of water, ions or solutes into the guard cell.

Three teams of investigators have recently reported analyses of stomatal deformations (Aylor et al. 1973, 1975; DeMichele and Sharpe 1973, 1974; Shoemaker and Srivastava 1973). All three groups model the guard cell as a Bernoulli-Euler beam. These models differ with regard to both assumed loading conditions and boundary conditions.

Aylor et al. assume the bending moment is proportional to the beam displacement and thereby model stomatal opening by beam buckling. DeMichele and Sharpe apparently take the bending moment to be constant along the length of the beam and, thus, appear to be modelling the case of pure bending. Shoemaker and Srivastava assume the bending moment to vary with the distance along the beam. In fact, they consider only half of a guard cell, and additionally require the displaced neutral axis to be symmetric about the middle cross-section of the beam. This requires that the slope and the shear force vanish at the beam's midpoint, but does not require that the bending moment vanishes there, a condition which they

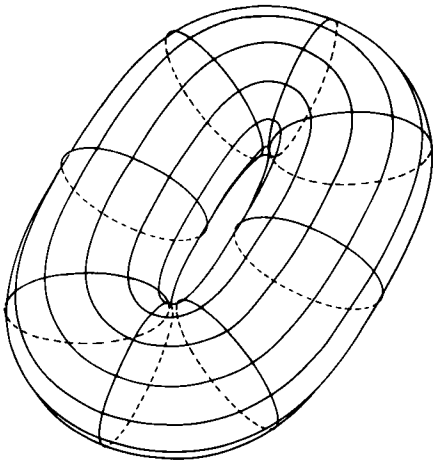

FIG. 3 Perspective view of undeformed guard cell pair.

apply, however.

Consider the choices of boundary conditions. Aylor et al. assume hinged supports for their beam model. This assumption yields zero displacements of the neutral axis (along the beam axis as well as perpendicular to the beam axis) at the ends of the guard cells, but allows rotations at the points where the cells join. In other words, the common surfaces at the ends of a guard cell pair are not required to remain in contact at all points. The rotations produce overlaps and gaps.

DeMichele and Sharpe adopt a curved beam model without employing curved beam theory. They assume that the neutral axis coincides with the concave surface of the beam. This assumption, as they indicate, is inconsistent with the use of the straight beam equation. Further, they do not discuss boundary conditions, but are apparently modelling a pure bending situation and thus are permitting rotations at the ends of the beam. Such rotations, as discussed above, would result in a gap at the common surfaces at the ends of the guard cells. Shoemaker and Srivastava set the displacement and the slope at the ends of the guard cell equal to zero.

Beam theory is based on the assumption that one of the three dimensions of a beam is large in comparison to the two remaining ones. The geometry of the stomate presents a guard cell which is only 3 to 4 times longer than it is wide or deep. Moreover, the value of the modulus of elasticity entering the beam equations refers only to the direction along the length of the beam. Hence, it seems appropriate to model the guard cells as orthotropic shells rather than beams.

The theory of elastic shells (Novozhilov (1959)) may be considered as a special case of the theory of elasticity, valid for elastic bodies which are surface-like in shape (i.e., which have relatively small thickness in comparison to their other dimensions). There are many different shell theories, most of which may be classified according to the following assumptions: (a) Linear versus nonlinear. The linear theory assumes that the deflections are small compared with the shell's thickness. This type of nonlinearity is called geometric. Another type of nonlinearity stems from nonlinear elastic material properties. (b) Thin versus thick. Thin shell theory assumes that the local thickness is small compared with the local (minimum) radius of curvature of the shell's middle surface. (c) Membrane versus bending. The membrane theory assumes that the shell in a moment-free state of stress. Moreover, elastic shell theories may be classified as isotropic, or anisotropic depending upon which version of Hooke's Law is utilized.

Aylor et al. (1973) state that stomatal opening requires the presence of radially arranged cellulose microfibrils and their model depends upon constraints on the length of the stomatal system, although neither the mechanical nor anatomical basis for the latter requirement in elliptical stomates is presented. They point out that the DeMichele and Sharpe model necessarily requires a changing pore length. Aylor et al. also conclude that the ventral wall need not be thicker than the dorsal wall for stomatal opening, but rather, it is a hindrance. The following analysis concurs with this view; but, it also indicates that radial micellation is not necessary and, in a sense, may also be considered a hindrance. However, the micellation, as will be detailed below, does produce a more favorable relationship for the opposing effects of guard cell and subsidiary cell pressures, especially for thin walls. If the balloon model of Aylor et al. had included thicker walls (in relation to the cross section of the guard cell), had completely eliminated end rotations, and had used a different (unstressed) initial configuration, perhaps less importance would have been assigned to micellae in determining pore size. DeMichele and Sharpe (1973) and Shoemaker and Srivastava (1973) included the effect of subsidiary cell influence while Aylor et al. (1973) did not. The shell model presented below also reveals that subsidiary cell pressure has a significant influence on the functioning of the stomate and on the shape of the deformed cross section, especially when

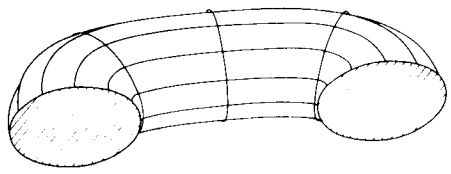

FIG. 4 Perspective drawing of a single guard cell.

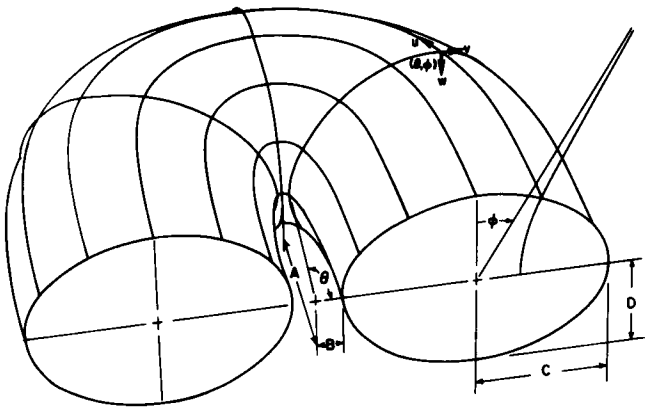

FIG. 5 Four parameters specify the undeformed geometry of the middle surface.

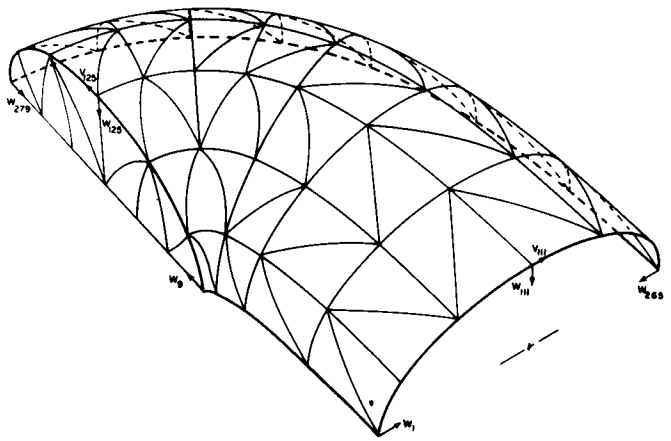

FIG. 6 Discretization used for one-fourth of a guard cell [perspective view].

the wall is thin.

FORMULATION OF ELASTIC SHELL MODEL

We shall now formulate a generic model of the elliptic-shaped guard cell which embodies the minimal biological detail necessary for an adequate representation of stomatal deformations. Fig. 3 shows the assumed initial unstrained configuration of the middle surface of the generic model of two guard cells. The middle surface of the shell is located halfway between the inner and outer surfaces of the (variable thickness) guard cell wall. The shape is constructed by revolving an ellipse (the generatrix) oriented perpendicular to the surface of the leaf, about an ellipse (the directrix) located in the plane of the leaf. The intersection of the ellipses, shown in Fig. 3, is always orthogonal. Fig. 4 shows one of the guard cells of Fig. 3. Elliptic plates are included in each end of the shell and are shown shaded in Fig. 4. The existence of such a common internal wall is inferred from Heath (1959a,b) who has shown that the two cells can be caused to act independently (by rupturing either a guard cell or a subsidiary cell).

The shape of the undeformed shell is uniquely defined (see Fig. 5) by the parameters A, B, C, and D which specify the four semi-axes of the ellipses. Two orthogonal curvilinear coordinate systems are required in the analysis — one for the elliptical torus and another one for the elliptical plate at each end of a guard cell.

The geometry of the middle surface of the curved portion of the shell (i. e., excluding the flat plate at the end) is defined by the following expressions for the Cartesian coordinates, x, y, z of any point on the middle surface of the shell in terms of the curvilinear surface coordinates, Θ, Φ.

$$x = \cos\Theta\left\{B + AC\left[1 + \sin\phi\right]\left[(A\cos\Theta)^2 + (B\sin\Theta)^2\right]^{-1/2}\right\} \quad \ldots\ldots [1a]$$

$$y = \sin\Theta\left\{A + BC\left[1 + \sin\phi\right]\left[(A\cos\Theta)^2 + (B\sin\Theta)^2\right]^{-1/2}\right\} \quad \ldots\ldots [1b]$$

$$z = D\cos\phi \quad \ldots\ldots [1c]$$

where $0 \leqslant \Theta \leqslant \pi/2$ and $-\pi/2 \leqslant \Phi \leqslant \pi/2$. (See Fig. 6).

The origin O of the xyz coordinate system coincides with the centroid of the pore. The theta coordinate locates the point of intersection of an elliptical cross section of the guard cell and the ellipse which forms the pore. The phi coordinate locates the position on the elliptical cross section. More specifically, phi locates the asymptote of a member of a system of confocal hyperbolas. (See Moon and Spencer 1961, p 204). Any point on the curved (middle) surface of Fig. 6 is uniquely specified by the (Θ, Φ) coordinates. The constant Θ curves are elliptical and the constant Φ curves are "elliptic-like" curves which correspond to constant elevation curves on the undeformed shell.

A different curvilinear coordinate system is used for the elliptic plates. It is defined as follows:

$$x' = a\cosh\eta\sin\Phi \quad \ldots\ldots [2a]$$

$$y' = a\sinh\eta\cos\Phi \quad \ldots\ldots [2b]$$

where $\eta_0 \leqslant \eta \leqslant 0$, $0 \leqslant \Phi \leqslant \pi$. The eta coordinate ranges over negative values in order to enable the coupling of the displacements of the plate and the shell at common node points, i. e., to obtain a common direction for positive displacements. One half of the interfocal distance, a, is related to the constants C and D in equation [1] as follows:

$$a = C/\cosh\left[\tanh^{-1}(D/C)\right] \quad \ldots\ldots [3]$$

Constant eta curves form a system of confocal ellipses. The $\eta = \eta_0$ curve coincides with the $\Theta = \pi/2$ curve. The degenerate ellipse $\eta = 0$ is the straight line connecting the two foci. The Φ and Φ coordinates coincide when $\Theta = \pi/2$.

This geometry was used in the finite element shell program developed at Cornell University by Thomas and Gallagher (1975), and subsequently extended by Kanodia (1976) and Mang, Kanodia and Gallagher (1976). The shell program uses linear bending theory for thin orthotropic shells.

The finite element method is a powerful numerical technique for obtaining approximate solutions to systems of partial differential equations, particularly for problems in engineering and mathematical physics (Gallagher 1975; Cook 1974; Huebner 1975; Segerlind 1976); its popularity and effectiveness is dependent upon the large size of the general-purpose, digital computers. The ease with which non-homogeneous, non-isotropic conditions (which are so prevalent in biology) can be treated is striking. Another attractive characteristic is that once fully tested and documented programs have been developed, a wide range of problems can be solved with very minimal programming by the user. On the other hand, the present liabilities of the method include the "massive input and output" of data and the requirement for a "large" computer.

An IBM 370/168 computer was utilized in the present study; a conversational time sharing system (Conversational Monitor System) was used to run a virtual machine under the Virtual Machine Facility operating system. The solution for each set of parameters involved the computation of an array of 115,000 double precision numbers which represent 695 simultaneous linear, algebraic equations with a semiband width of 157. A total processing time (CPU) of 2 min and 17 sec was required to run the FORTGI compiled modules in the virtual machine using an available memory of 1.5 megabytes.

One of the first surveys of finite element representations for thin-shell analysis was published by Gallagher (1969). A significant number of other surveys, including the ones by Dawe (1971), Forsberg and Hartung (1971), Bushnell (1974) and Gallagher (1975), have since appeared. Most recently, a book, edited by Ashwell and Gallagher (1976), devoted exclusively to the topic of finite elements for thin shells and curved members, has been published.

There are three distinct modes of finite element representation of thin shell structures: (a) flat finite elements, based on the theory of thin plates, yielding 'faceted'-type models of shells, (b) curved finite elements, formulated on the basis of non-shallow and shallow, respectively, thin-shell theory and (c) three-dimensional (solid) finite elements, formulated on the basis of three-dimensional theory of elasticity

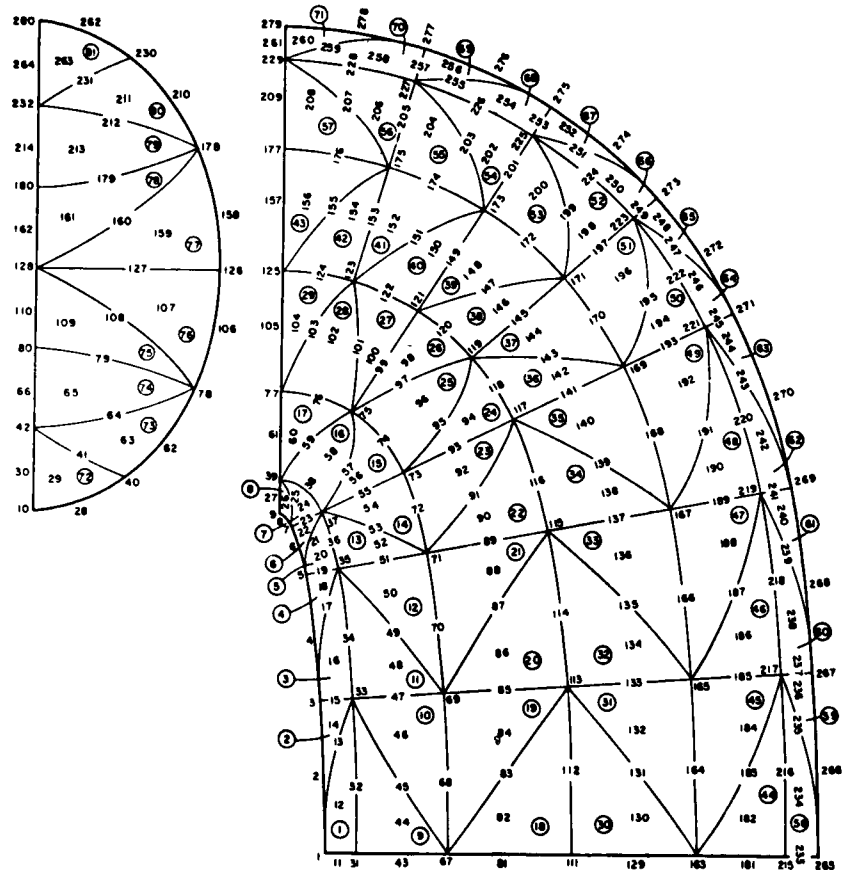

FIG. 7 Nodal and element [circled] numbering scheme used for shell and plate [orthographic view].

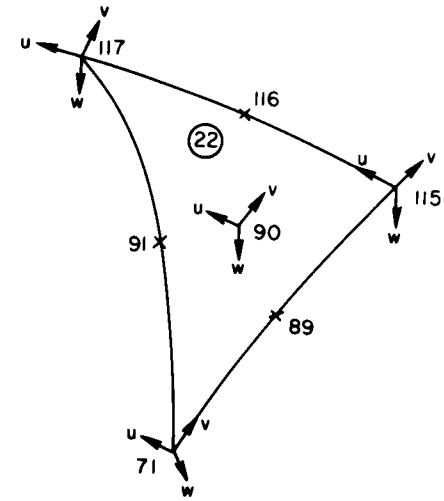

FIG. 8 A typical doubly curved triangular shell element. The partial derivatives of the displacement components are not shown.

(Gallagher 1976).

The aforementioned finite element shell computer program was developed along the lines of nonshallow thin-shell theory (mode (b)), using a formulation based on assumed displacement fields for the individual finite elements (Thomas and Gallagher 1976). In general, the advantages of mode (b) of finite element representation of thin shell structures over modes (a) and (c) exceed its disadvantages.

The success of this approach depends on the degree of satisfaction of the requirements of: (a) zero strain energy under rigid body motion of the shell, (b) inclusion of states of deformation yielding constant strain, (c) interelement continuity of displacements and slopes (C^1 continuity) (Gallagher 1976). In general, it is impossible to satisfy all three requirements.

For the present case, C^1 continuity is satisfied exactly. The other two requirements are not met. However, the choice of cubic polynomials as displacement functions often enables approximate satisfaction of the requirements (a) and (b). The quality of the approximation increases with the refinement of the finite element mesh.

Discretization of the Guard Cell

The finite element method is based upon the judicious subdivision of a given domain into a number of subdomains — the individual finite elements. Simple approximations are made for the states of deformation within the individual finite elements. After forming so-called stiffness matrices for the individual elements, these matrices are placed into the global stiffness matrix. This procedure is termed the assemblage of the finite elements. Thereafter, appropriate boundary and interelement continuity conditions are specified.

The assemblage of doubly-curved triangular finite elements shown in Fig. 6 was employed for the analysis. The size of the elements was reduced in the regions of large initial curvature and the arc lengths of the three edges of the elements were chosen to be approximately equal.

As an aid in the further elaboration of the coordinate systems used, refer to the numbered points (1-280) on the orthographic projection of the shell (Fig. 7). The curves Θ = constant appear as straight lines in the direction of the micellae. The line bounded by nodes 1 and 265 corresponds to $\Theta = 0$ and the line terminated by nodes 9 and 279 corresponds to $\Theta = \pi/2$. The ellipse-like curves correspond to curves Φ = constant. The curves terminating at nodes 1 and 9, 111 and 125, and 265 and 279 correspond to $\Phi = -\pi/2$, 0, $\pi/2$, respectively.

For the elliptic plate the constant η curves constitute a set of confocal ellipses whereas the constant Φ curves form a set of confocal hyperbolas. The lines joining nodes 10 to 42 and 232 to 280 corresponds to $\Phi = 0$, and $\Phi = \pi$, respectively. Nodes 42 and 232 are connected by a degenerate ellipse. Nodes 42 and 232 were initially selected to coincide with the foci. Subsequently, however, an ellipse with η slightly different than zero was chosen in order to circumvent numerical problems stemming from singularities associated with the foci.

The nodal numbering scheme shown in Fig. 7 was chosen to keep as small as possible the bandwidth of the system of linear algebraic equations to be solved. In this context, note that the computer time required for the solution of the system of simultaneous equations is approximately proportional to the square of the bandwidth.

As shown in Fig. 8, each element has seven nodes — one at each vertex, one at each mid-side and one at the centroid. Each vertex node has nine degrees of freedom or unknowns — 3 orthogonal components of the displacement vector (u, v, w), one of which, w, coincides with the direction of the normal to the surface; and partial derivatives of these displacements with respect to the two orthogonal curvilinear coordinates. The other two components of the displace-

ment vector, u and v, are located in a plane tangential to the middle surface of the shell. u is tangent to a parametric line Φ = constant, while v is tangent to a parametric line Θ = constant. The remaining unknowns, that is, the three orthogonal components of displacement, specified at the centroid of the element as well as the so-called Lagrangian multipliers, associated with mid-side node points and representing average normal bending moments, serve the purpose of improving the performance of the finite element (Mang and Gallagher 1976). The element numbers, arbitrarily assigned to the individual elements, are circled in Fig. 7.

Boundary Conditions

Since the state of deformation of the shell is symmetric with respect to the boundary lines shown in Fig. 7, symmetry conditions have been specified for the vertex nodes located on these lines. Thus, for the vertex nodes situated on the symmetry lines $\Theta = 0$ and $\Theta = \pi/2$, the following degrees of freedom were set equal to zero: u, $\partial u/\partial\Phi$, $\partial v/\partial\Theta$, $\partial w/\partial\Theta$. Similarly, for the vertex nodes located on symmetry lines $\Phi = -\pi/2$ and $\Phi = \pi/2$, $\partial u/\partial\Phi$, v, $\partial v/\partial\Theta$ and $\partial w/\partial\Phi$ were set equal to zero.

Since the elliptic plate at the end ($\Theta = \pi/2$) does not protrude into either of the guard cells in the pair, the transverse displacement of the plate, w, was set equal to zero. However, the plate was allowed to stretch, thereby providing some elastic constraint to the motion of the shell in the plane of the plate. The components of the displacement vector at the perimeter of the plate were set equal to the appropriate components of the displacement vector of the shell. Since the plate was not prevented from moving in its own plane, the stomatal pore could assume a length consistent with the elastic behavior of the entire shell.

Shell Thickness

The shell thickness was specified at each of the vertex nodes. The thickness was assumed to vary linearly with Θ and Φ within an element of the finite element mesh. In addition to the assumption of a thin shell, the wall thickness in the vicinity of $\Theta = \pi/2$, $\Phi = -\pi/2$ was limited to prevent overlap with the mirror image portion of the shell for certain values of the assumed initial configuration (i. e., A and B, see Fig. 5).

Pressure Loads

The hydrostatic pressure inside the guard cell was assumed to act uniformly and normal to the middle surface of the shell at every point (see Fig. 13). Due to symmetry at the elliptic plate, an equal and opposite pressure was assumed (i. e., the net pressure was taken as zero). The adjacent epidermal cell was assumed to provide a uniform pressure load around the entire outer perimeter of the guard cell. The net pressure in that region ($\Phi = \pi/2$ to $\pi/6$) was used as the pressure load. To avoid an abrupt change in loading, the pressure difference was tapered to the top of the guard cell ($\Phi = \pi/6$ to 0).

Although the net pressure loading on the shell is assumed to act at the hypothetical middle surface (of zero thickness), a "mechanical advantage" for the subsidiary cell was found. This effect is still present when the opposing pressures act on the middle surface. The explanation is a matter of shell geometry and material properties and of the portions of the shell on which the pressures are applied.

No other influence of the adjacent cells was included. As mentioned earlier, there appear to be hinge-like connections between the guard cell and the adjacent epidermal cells (Meidner and Mansfield 1968) which have not been considered in this model. The computed deformation in all cases considered showed minimal displacement in the plane of the leaf in the vicinity of the epidermis, thereby providing additional justification for the assumption.

This result is also intuitively satisfying, since the stomate would be able to open and close with very little mechanical disturbance to the rest of the leaf.

NUMERICAL EXPERIMENTS

In the absence of reliable experimental parameters for the model, e. g., moduli of elasticity, Poisson's ratios and thickness, we are limited to an examination of trends. Nevertheless, some rather important new perspectives can be added to the hypotheses concerning stomatal mechanics. In particular, we shall comment upon the influence of guard cell geometry, wall thickness, micellae, guard cell and subsidiary cell pressures and the cell walls where the guard cells of a pair join. In order to be able to comment upon a hypothetical constraint on pore length, that

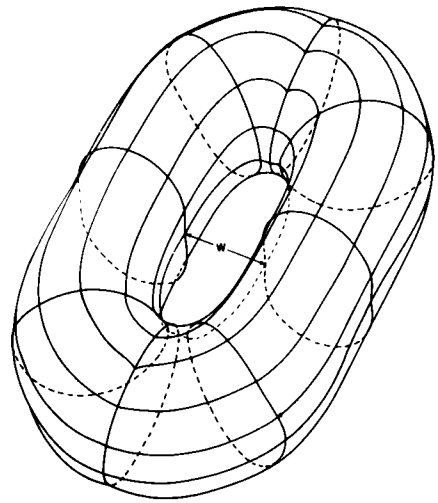

FIG. 9 Perspective drawing of deformed guard cell pair.

condition was also included in some cases.

Guard Cell Geometry

If an isotropic circular torus is considered, (i.e., if A = B,C = D) and if $\nu = 0.39$ and $P_S = 0$, we find that the circular pore *decreases* in size when P_g is increased unless $B/C > 1.77$, e. g., if a "hula-hoop" like configuration is assumed. (See Appendix B). Having the pore open under drought (high water stress conditions) is, of course, unacceptable and is also contrary to what has been reported in the literature. The turgor operated valve, i. e., the stomate, is an example of a normally-closed, fail-safe valve. The geometry of the stomate is an important factor of its operation.

The cross-sectional geometry of the guard cell is also important. If the initial configuration of the cross-section is circular or elliptical with the major axis in the direction perpendicular to the leaf (rather than with the minor axis perpendicular to the leaf), changes in cell volume and pore size depend more heavily upon cell wall stretching than upon shape changes.

Guard Cell Wall Thickness

Fig. 9 shows the deformed shape of a guard cell, the initial configuration of which is that given in Fig. 3. The cell wall has a uniform thickness (which extends equal distances on each side of the surface depicted). For reasonable estimates of the parameters, the guard cell does open; unequal thickening of the dorsal and ventral walls is not required. The predicted deformations may be compared to the ones for the fully opened cucumber stomate in Fig. 2. The walls forming

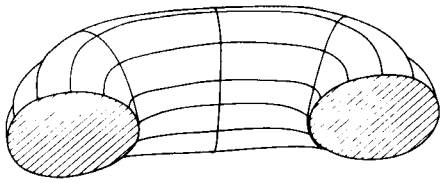

FIG. 10 Perspective drawing of deformed guard cell.

the aperture appear to be nearly vertical in both cases. (See Fig. 10 also). The surface of the guard cell has bulged upward, i. e., out of the plane of the leaf. At each end of the aperture the bulge has been diminished by the presence of the "elliptic plate" where the two guard cells join. Finally, the wall of the guard cell along the side ($\Theta = 0$, $\Phi = \pi/2$) (cf. Fig. 9) bends towards the interior of the guard cell — rather than into the adjacent cell. The corresponding motion, of course, is not visible in Fig. 2.

Raschke (1975) has noted that according to measurements in epidermal strips, the width and depth of guard cells in *Vicia faba* and the length of the stomatal apparatus change very little. Meidner and Mansfield (1968, p. 12) have stated that "the overall width of stomata increases as they open, but the width of individual guard cells changes only in some stomata; frequently, when it does, the maximum width is attained when the pore is about half open, decreasing towards its original width with further opening. Reliable measurements of the changes in depth of stomata during the opening and closing process are not available but these changes must presumably occur when the guard-cell volume changes without appreciable changes in the length and width." The out-of-plane motion was always present in the calculations and deserves further experimental study.

Whether the guard cell has been observed to "bulge" into the epidermal cells or whether this motion is just an inference from the thick-wall hypothesis is not clear from the literature (e. g., Meidner and Mansfield, p. 15). In all cases computed by us, the wall at $\Theta = 0$, $\Phi = \pi/2$ moved away from the subsidiary cell when either P_g or P_s was increased. The stomate model, when viewed normal to the plane of the leaf, has the appearance depicted by the orthographic view of Fig. 11. The dashed lines depict the initial configuration for the pore ($\Phi = -\pi/2$), the outermost perimeter of the guard

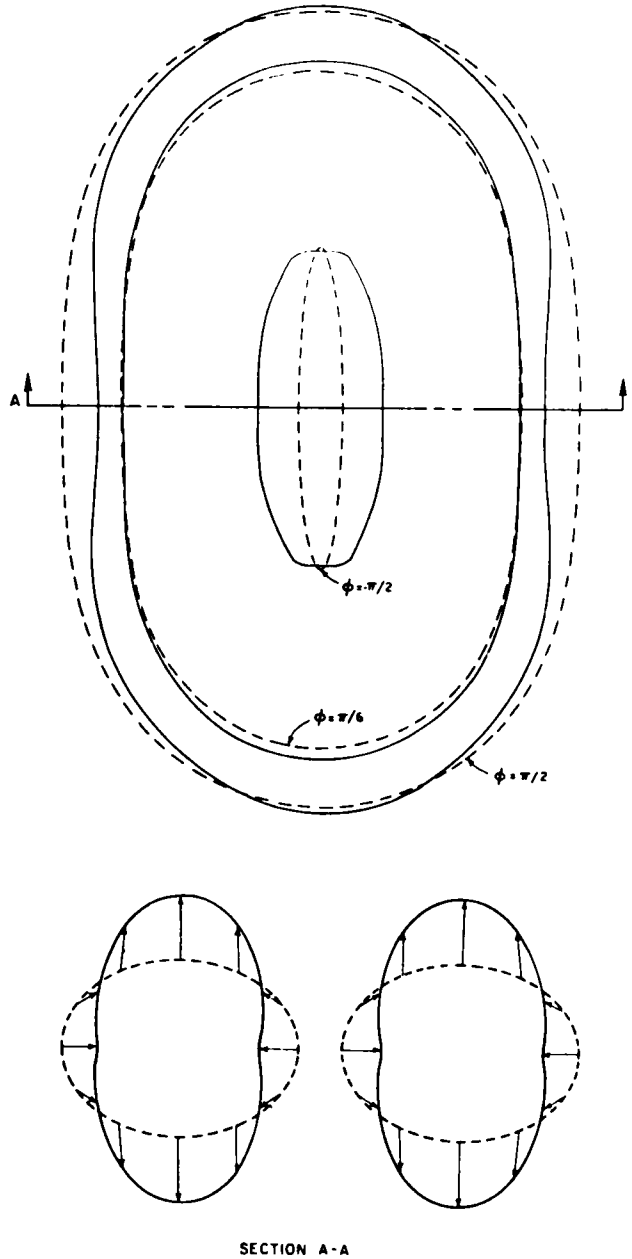

FIG. 11 Orthographic projections of the undeformed [dashed lines] and deformed [solid lines] stomate.

cell ($\Phi = +\pi/2$) and the approximate location of the attachment of the epidermal cell to the guard cell ($\Phi = \pi/6$); the solid lines show the corresponding deformed configuration when $P_g = 6 \times 10^5$ Pa and $P_s = 1 \times 10^5$ Pa. [Note: 10^5 Pascals = 1 bar; 1 $\mu N/(\mu m)^2$ = 10 bars]. Observe that the lateral motion at the approximate juncture of the guard cell and epidermis was virtually zero. However, if one could see through the epidermis, the outer perimeter at $\Theta = 0$ would be seen to bulge towards the interior of the guard cell. The bulge would be even more pronounced if the dorsal wall common to the two types of cells is thinner than the ventral wall at the pore. While a thin dorsal wall *may* facilitate transport between the subsidiary and guard cells and a thick (cutinized) ventral wall *may* serve to protect the guard cell (e. g. from water vapor loss through the wall to the atmosphere or from entry of liquid water into the stomatal cavity) the variable wall thickness does not appear to relate directly to the structural requirements for opening. Indeed, the deformed cross section corresponding to a uniformly thick (2 μm) shell (see Fig. 11 bottom) is noticeably more realistic than it would be for the undeformed cross section of Fig. 13. In this latter case the deformation of the thin portion of the shell becomes excessive.

The variable wall thickness of Fig. 13 is 2 μm at the pore (on the left $\Phi =$

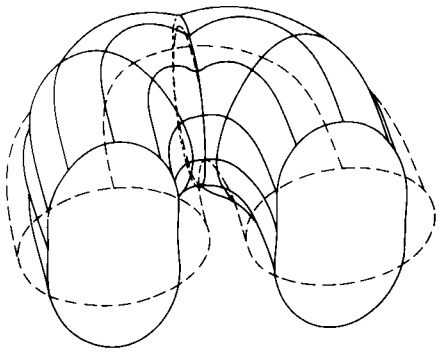

FIG. 12 Comparison of deformed [solid] and undeformed [dashed] guard cells.

$-\pi/2$), increases to 3 μm at the lip ($\Phi = -\pi/6$) and eventually decreases to 1 μm at the epidermal cell ($\Phi = \pi/6$ to $\Phi = 0$). The aperture width as a function of P_g and P_S was virtually unchanged compared to a uniform wall thickness of 2 μm.

Comparison of two uniformly thick walls of 2 μm and 0.5 μm reveals that membrane action predominates when the wall becomes too thin and the desired sensitivity of pore width to P_S is lost.

Fig. 12 shows the deformed case (solid lines) for the uniformly 2μm thick shell superimposed on the undeformed case (dashed lines). The aperture has experienced virtually no change in length, although it has been free to change as dictated by the motion of the rest of the shell. As discussed in the following, the small increase or decrease in the length of the aperture depends upon the parameters used. The cross-sectional changes are apparent, as is the change in aperture width. The cross-section of the elliptic plate changes only slightly.

Micellae (Radial Stiffening)

The effect of the micellae was modelled by assuming orthogonally anisotropic (orthotropic) elastic properties of the shell material. The force required to stretch a square section over a unit distance would be much greater in the direction of the micellae than perpendicular to the orientation of the micellae. Rather than two independent elastic constants (e. g., Young's modulus, E, and Poisson's ratio, ν) we now have three — that is, Young's modulus perpendicular to the micellae, E_Θ; Young's modulus in the direction of the micellae, E_Φ; and Poisson's ratio in the direction of the micellae, ν_Φ. [The two other typical constants, ν_Θ and $G_{\Theta\Phi}$ may be obtained from the three specified ones (Huber 1925, Lekhnitskii 1968. In particular, we used

$$E_\Theta \nu_\Phi \mu = E_\Phi \nu_\Theta \text{ and}$$

$$G_{\Theta\Phi} = (1/2)(E_\Theta E_\Phi)^{1/2} [\, 1 - (\nu_\Theta \nu_\Phi)^{1/2}] / [1 - \nu_\Theta \nu_\Phi].$$

Consider, for example, a shell with cross section of Fig. 13 for which E_Θ and P_S are held constant. Then an increase in E_Φ (micellae stiffness) will require a larger P_g to achieve a given aperture width W. Moreover, the ratio of the sensitivity of the aperture width to P_S and P_g (i.e., a_S/a_g of equation [4] is changed from -0.97 to -1.51 and to -1.91 as the E_Φ/E_Θ ratio changes from 1:1 to 5:1 and to 10:1. Therefore, increasing the strengthening effect of the micellae has the effect that a unit increase in P_S causes a relatively larger decrease in aperture than the increase in aperture caused by a unit increase in P_g. We conjecture that this characteristic may be especially important in the proper functioning of the stomate as a turgor actuated valve in the water and carbon dioxide level control systems.

Pore Width Related to Turgor Pressures P_g and P_S

As a direct consequence of the assumed linearity of the analysis, each freedom at a vertex node can be represented as a linear combination (multilinear function) of P_g and P_S. For example, the transverse component of the displacement vector at node i is obtained as

$$w_i = a_g P_g + a_S P_S \quad \ldots\ldots\ldots\ldots \quad [4]$$

where a_g and a_S are influence coefficients which can be found from two load cases. Agreement with this multilinear relationship was verified for each degree of freedom at the vertex nodes (Snedecor and Cochran 1967). The computed values for three different load cases were used in the standard least squares analyses and the regression values were found to agree with the results for the two additional load cases used.

Since the multilinear relationship has been validated, the influence coefficients may be conveniently obtained without the use of the regression technique by simply choosing unit pressure loads in two load cases in the finite element analysis, i. e., $(P_g, P_S) = (1,0)$ and $(0,1)$. The w_i axis intercept is zero, since w must be zero when both P_g and P_S are zero. The signs of a_g and a_S may be positive or negative. As a special case of equation [4], consider node 1. In this case, w_1 is

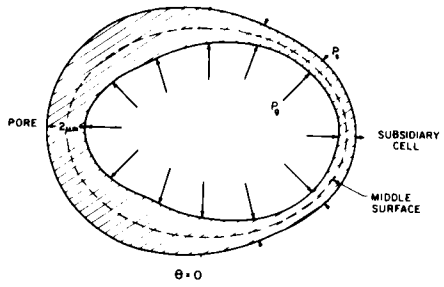

FIG. 13 Variable thickness cross section of guard cell used in sets 4, 5 and 6.

just the increase in the half width of the pore; a positive w_1 implies a wider aperture.

There are three important consequences of this observation. First, a set of coefficients (a_g, a_S) for each node may be found. The deformed shape of the guard cell is then easily obtained for any P_g, P_S combination (for the prescribed set of parameters). Second, these coefficients may be used to summarize and to study the influence of changes in the various parameters, such as E_Φ/E_Θ. (See Table 1, Pressure Influence Coefficients for Selected Displacements.) A detailed discussion will be presented below. In passing, however, we note that the tabulated results may be immediately generalized to apply for any E_Θ, for the indicated E_Φ/E_Θ ratio. The tabulated entries correspond to a plausible, but arbitrarily chosen E_Θ, denoted here as E_{ref}. Equation [4] may be generalized as follows:

$$w_i = (a_g P_g + a_S P_S)(E_{ref}/E_\Theta) \quad \ldots\ldots \quad [5]$$

E_Θ may then be deleted from the list of parameters implicitly affecting the influence coefficients. The remaining parameters characterize (a) the initial configuration of the middle surface [A, B, C and D], (b) the wall thickness at each node and (c) the material properties of the shell [E_Φ, E_Θ, ν_Φ] and of the elliptic plate [E_η, E_Φ, ν_Φ].

Third, the aperture width at node 1 is simply a special case of the above. In short, the full width of the aperture should be a multilinear function of P_g and P_S.

The width of the aperture, denoted by upper case W, may be written as

$$W = b_0 + b_g P_g + b_S P_S \quad \ldots\ldots\ldots \quad [6]$$

which is valid only for non-negative widths, i. e., $W \geq 0$, where the *influence coefficients b_g and b_S* are twice the coefficients of equation [4] obtained from the shell analysis since the

walls of the pore move in opposite directions. A non-zero intercept b_0 is possible since the initial configuration and the shell thickness may be such that the pore is either lightly or tightly closed for $P_g = P_s = 0$. For most practical situations, b_g is positive and b_s is negative; since the hydrostatic (turgor) pressures are non-negative, P_g and P_s need not be zero for the stomate to be closed.

We shall now show that data obtained using the plasmolytic method (Glinka 1971) and a direct method (Edwards et al. 1976) are fully compatible with equation [6].

Consider the data presented by Glinka in 1971. The plasmolytic method was used to determine the turgor pressure of the guard and adjacent epidermal cell. Stomatal aperture was measured under steady state conditions. Specifically, the turgor pressure of the "subsidiary" cell was approximately 5.3 atm below the turgor pressure of the guard cell over a range of water potentials as shown in Fig. 14 (after Glinka). The aperture increased with a decrease in P_g! Note though, that P_s was simultaneously decreased. After P_s reached zero, P_g was decreased further with an accompanying decrease in aperture.

Two of Glinka's observations will now be re-interpreted using the insight developed in the course of this investigation. First, Glinka concludes that, "at least in *Vicia faba*, the pressure of the epidermal cells predominates in determining the stomatal aperture." Second, Glinka points out (cf. Fig. 14) that the maximum stomatal aperture did not occur at maximum P_g, but when P_s was nearly zero (i. e., near incipient plasmolysis) and P_g was approximately 5 atm.

Consider the following two procedures for calculating b_0, b_g, b_s. For the situation in which the epidermal turgor pressure P_s is zero, we have from equation [6]

$$\partial W/\partial P_g \Big|_{P_s = 0} = b_g \quad \ldots\ldots\ldots \quad [7]$$

obtained from the right half of Fig. 14 where $\psi = -7 \times 10^5$Pa and $\psi = -9 \times 10^5$Pa. The left half of the figure was obtained under conditions of approximately constant $\Delta P = P_g - P_s$. By addition and subtraction of $b_g P_s$ in equation [6]

$$W = b_0 + b_g (P_g - P_s) + (b_g + b_s) P_s \quad \ldots\ldots\ldots\ldots\ldots\ldots \quad [8]$$

Clearly, the pore width does *not* depend solely upon the pressure difference between the guard cell and the subsidiary cell, $(P_g - P_s)$, as frequently stated in the literature (e. g. Stålfelt 1966, Edwards et al. 1976) unless $(b_g + b_s) = 0$. From the definition of the partial derivative we obtain

$$\partial W/\partial P_s \Big|_{(P_g - P_s) = \text{constant}} = (b_g + b_s) \quad \ldots\ldots\ldots\ldots\ldots\ldots \quad [9]$$

$$= (6.7 - 14.4)/(6.5 - 0.9) = -1.4\ \mu m/(10^5 Pa)$$

using the values at $\psi = -6 \times 10^5$Pa and $\psi = 0$ on the left portion of Fig. 14.

Using equations [7] and [9] we find

$$b_s = -4.3\ \mu m/(10^5 Pa) \quad \ldots\ldots\ldots \quad [10]$$

Now determine the b_0 value by requiring, for example, that the equa-

TABLE 1. PRESSURE INFLUENCE COEFFICIENTS FOR SELECTED DISPLACEMENTS.

Set		1	2	3	4	5	6	7	8	9	10	11	12	13	14
Thickness, μm		2	2	2	var.	var.	var.	0.5	0.5	2	2	2	2,1	2,1	2,1
E_ϕ/E_Θ		1	5	10	1	5	10	1	10	1	10	1	1	5	5
Notes										con-strained	con-strained				con strained
w_1	a_g	0.117	0.060	0.043	0.119	0.061	0.043	2.334	0.891	0.105	0.040	0.153	0.214	0.073	0.091
	a_s	-0.115	-0.093	-0.082	-0.115	-0.092	-0.081	0.260	-0.161	-0.111	-0.078	-0.137	-0.171	-0.124	-0.115
	a_s/a_g	-0.98	-1.55	-1.90	-0.96	-1.51	-1.91	+0.11	-0.18	-1.06	-1.96	-0.89	-0.80	-1.71	1.26
w_9	a_g	-0.012	-0.005	-0.002	-0.011	-0.003	0.000	-0.128	-0.046	0	0	-0.004	-0.004	0.044	0
	a_s	0.005	0.003	0.001	0.004	0.002	-0.001	0.013	0.018	0	0	0.027	0.033	0.013	0
	as/ag	-0.44	-0.66	-0.61	-0.39	-0.57	-8.59	-0.10	-0.38			-6.45	-7.46	0.30	
v_{111}	a_g	-0.007	0.018	0.020	-0.029	0.006	0.011	-0.483	-0.113	-0.005	0.017	-0.022	-0.068	-0.015	0.007
	a_s	-0.159	-0.108	-0.090	-0.154	-0.108	-0.090	-1.173	-0.597	-0.158	-0.086	-0.168	-0.207	-0.136	-0.135
	a_s/a_g	23.96	-5.96	-4.54	5.29	-19.54	-8.49	2.43	5.29	28.98	-4.93	7.63	3.06	8.80	-17.5
w_{111}	a_g	-0.248	-0.072	-0.039	-0.345	-0.111	-0.062	-4.096	-1.277	-0.232	-0.037	-0.313	-0.570	-0.164	-0.158
	a_s	-0.025	-0.014	-0.008	-0.031	-0.021	-0.014	-0.601	-0.346	-0.029	-0.009	-0.019	-0.015	-0.014	-0.021
	a_s/a_g	0.10	0.19	0.20	0.09	0.19	0.22	0.15	0.27	0.13	0.23	0.06	0.03	0.09	0.13
v_{125}	a_g	0.011	0.010	0.009	-0.012	0.009	0.008	0.067	0.048	0	0	0.027	0.029	0.051	0
	a_s	-0.003	-0.008	-0.009	-0.002	-0.007	-0.008	-0.000	-0.030	0	0	-0.020	-0.033	-0.066	0
	a_s/a_g	-0.27	-0.78	-0.97	-0.017	-0.75	-0.97	0.01	-0.61			-0.73	-1.14	-1.30	
w_{125}	a_g	-0.019	-0.009	-0.007	-0.018	-0.009	-0.006	-0.060	-0.022	0	0	-0.241	-0.371	-0.095	0
	a_s	0.001	0.000	-0.000	0.000	-0.001	-0.001	0.004	0.002	0	0	-0.026	-0.044	-0.066	0
	a_s/a_g	-0.08	-0.02	0.02	-0.01	0.12	0.18	-0.06	-0.011			0.106	0.119	0.70	
w_{265}	a_g	0.121	0.022	0.003	0.358	0.114	0.058	3.101	1.047	0.105	0.004	0.183	0.592	0.177	0.148
	a_s	0.168	0.117	0.096	0.131	0.117	0.098	-0.070	0.579	0.172	0.092	0.173	0.131	0.132	0.140
	a_s/a_g	1.40	5.33	36.66	0.36	1.03	1.69	-0.02	0.55	1.64	23.69	0.95	0.22	0.75	0.95
w_{279}	a_g	-0.010	-0.007	-0.006	-0.008	-0.006	-0.005	-0.040	-0.020	0	0	0.052	0.172	0.012	0
	a_s	0.006	0.007	0.007	0.004	0.005	0.006	0.007	0.019	0	0	0.048	0.059	0.125	0
	a_s/a_g	-0.59	-0.97	-1.17	-0.45	-0.91	-1.14	-0.18	-0.96			0.92	0.343	10.41	

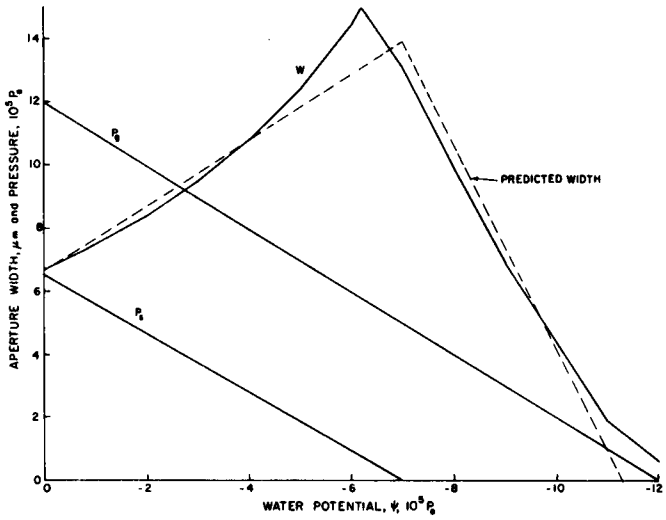

FIG. 14 Measured aperture width, predicted aperture width, guard cell turgor pressure, and subsidiary cell pressure as a function of water potential [adapted from Glinka].

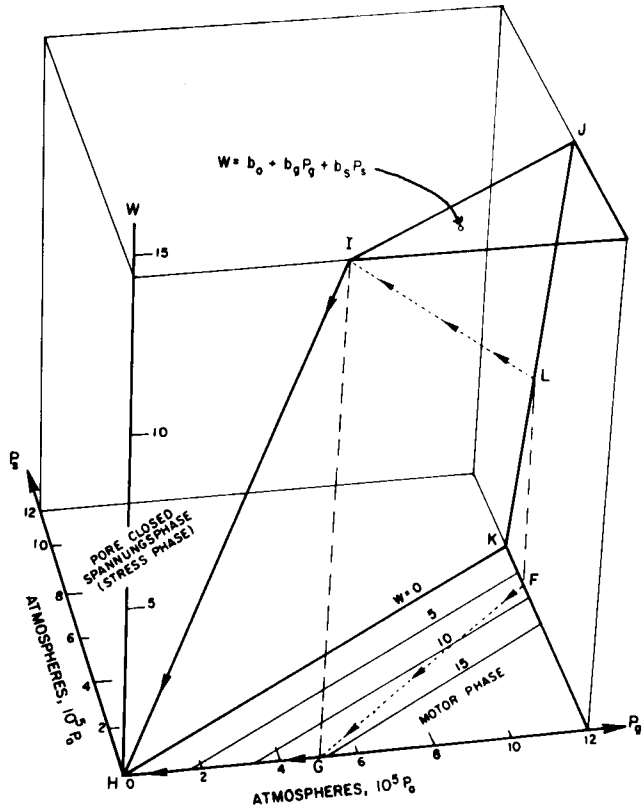

FIG. 15 Perspective view of relationship of aperture width to guard cell and subsidiary cell pressures.

tions agree exactly for pure water (ψ=0). This gives

$$b_0 = 6.7 - (2.9 * 12 - 4.3 * 6.5) = -0.15\ \mu m$$

Then

$$W = -0.15 + 2.9\ P_g - 4.3\ P_s \quad \ldots \quad [11]$$

provided $W \geqslant 0$ and where the units are μm and 10^5Pa. Using these values of b_0, b_g, b_s, the predicted values of W have an error of less than would occur by an uncertainty of 0.5 x 10^5 Pa in the value of P_g. A unit change in P_S has an influence that is larger in absolute value than that for a unit change in P_g and is of opposite sign. However, the question of which pressure predominates depends upon the actual range of pressures in P_g and P_S under normal conditions. Rather than conclude that "...the pressure of the epidermal cells predominates in determining the stomatal aperture," a more precise statement would be that the decrease in width for a unit increase in P_S, if P_g is held constant, is greater in absolute value than the increase in width for a unit increase in P_g, if P_S is held constant. The idea can be expressed very concisely in mathematical form:

$$\text{antagonism ratio} = \alpha = -(\partial W/\partial P_S)_{P_g} / (\partial W/\partial P_g)_{P_s} = -(b_s/b_g) \quad \ldots\ldots\ldots\ldots\ldots\ldots\ldots \quad [12]$$

We have coined the term "antagonism ratio" in honor of von Mohl who in 1856 recognized the antagonism between the guard cells and epidermal cells. [Translation from von Mohl's German language paper: "Therefore, it is clear that for Amaryllis, the opening and closure of the stomate does not depend solely upon the motion of the guard cells but also upon the antagonism between the guard cells and the epidermal cells."]

From equations [7] and [10] the antagonism ratio for *Vicia faba* appears to be approximately 1.5, a result which compares favorably with a 2 μm shell with $E_\Phi/E_\Theta = 5$, which [set 2, Table 1] has an antagonism ratio of 1.55.

An alternate derivation which considers the slight (P_g-P_S) variation in Fig. 14 is included in Appendix A.

The more traditional least squares method may be used if the original data are available. If (P_g, P_S, W) "data" are obtained from Fig. 14 at ψ = 0, -1, . . . -11 the following multilinear expression results:

$$W = 1.65 + 3.11\ P_g - 4.47\ P_s\ , \text{provided } W \geqslant 0 \quad \ldots\ldots\ldots\ldots\ldots\ldots\ldots \quad [13]$$

The predicted values, shown in Fig. 14, are in error by less than 0.5 μm for widths less than 10 μm and the maximum relative error for the larger apertures is less than 10 percent. The multiple correlation coefficient (Snedecor and Cochran 1967, p. 402) for these "data" is R = 0.99. This error is clearly within the limits of precision of the turgor pressures. The antagonism ratio, a, is 1.44.

Fig. 15 shows a perspective drawing of the multilinear relationship of P_g, P_S and the aperture width (i. e., plane HIJLK), using the coefficients of equation [11] obtained from the Glinka data. The ψ = 0 condition for pure water is given as point F (P_g = 12, P_S = 6.5) and corresonds to an aperture width given by point L. Now P_g and P_S are decreased but the difference is held constant. See line FG. The aperture therefore increases to point I along line LI on the HIJLK plane. Next P_g is decreased further while P_S remains at zero and the aperture decreases along path IH. From Fig. 15 it is clear that the aperture in our model behaves as reported by Glinka.

The contour lines W = 0, 10, 15 are shown projected onto the P_gP_S plane and the increase in aperture with decreasing P_g (when P_g-P_S = constant) is obvious, as is the fact that the largest aperture occurs at point G (i.e., point I on the plane HIJLK).

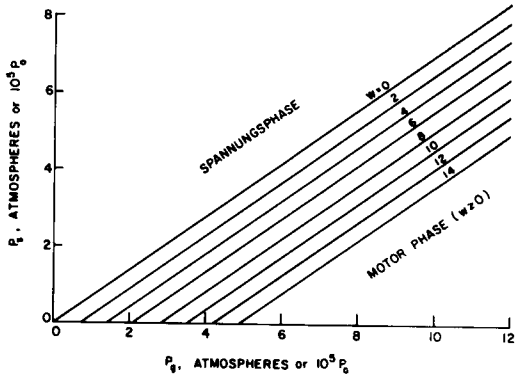

FIG. 16 Constant aperture curves on P_gP_s plane.

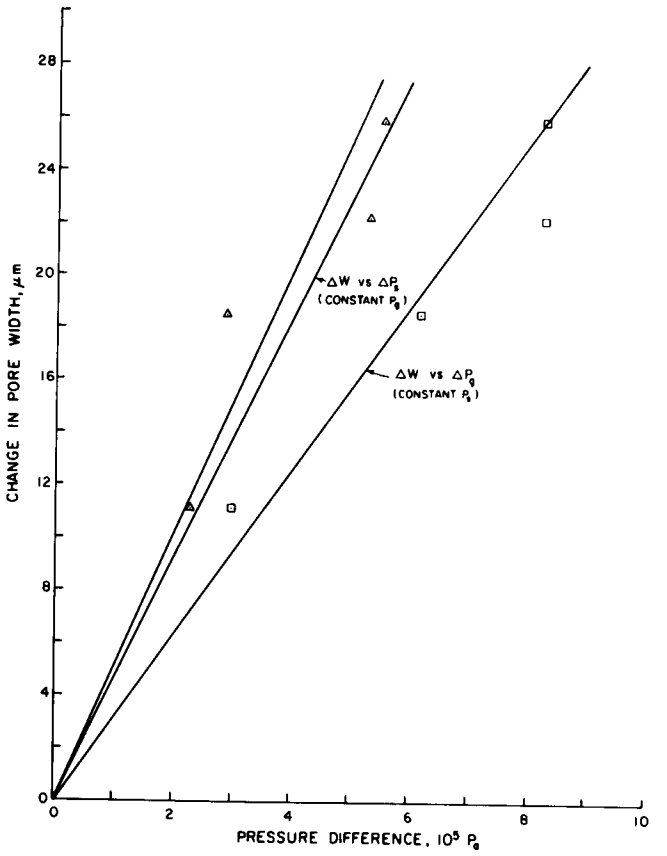

FIG. 17 Direct measurements of turgor pressure relationships [from Edwards et al. data].

However, for P_S = constant, note that W would increase as P_g increases.

The aperture width contours are shown again in Fig. 16 in a form which is more convenient for estimating aperture for any point on the P_gP_S plane. Any P_g,P_S coordinate to the left of the W = 0 line corresponds to a closed aperture. From Fig. 16, it is clear that the greater the normal distance from the W = 0 line, the greater the aperture.

Raschke (1975) has suggested that the plasmolytic method is dependent upon the time permitted for plasmolysis. Much higher osmotic values are obtained for shorter times in the plasmolized state. If the difference is due to solute movement across the cell wall, we conjecture that b_g and b_S coefficients are related to the structural properties and would be unchanged. In other words, the same aperture prediction relationship should result. This means, for example, that if P_g is increased from 8 to 40 and P_S is increased from 2.7 to 25, the same aperture width results using equation [13].

Recently, direct measurements of the turgor pressure in guard cells and subsidiary cells have been made by Edwards, Meidner and Sheriff (1976). Fig. 17 based upon their data shows (i) the increase in stomatal width in *Tradescanta virginiana* when P_g is externally increased while P_S is held constant with a hollow water-filled needle inserted in the subsidiary cell and (ii) the decrease in stomatal width when P_S is increased, while P_g is held constant with a hollow water-filled needle inserted in the guard cell. This experiment may be interpreted quite simply in terms of equation (6). Using a least squares regression through the origin for the lower curve we obtain

$$b_g = \partial W/\partial P_g \Big|_{P_S = \text{constant}}$$

$$= \Delta W/\Delta P_g = 3.12\ \mu m/10^5 Pa \quad \ldots\ldots\ldots\ldots\ldots\ldots\ [14]$$

For the upper curve we obtain

$$b_S = \partial W/\partial P_S \Big|_{P_g = \text{constant}}$$

$$= 5.01\ \mu m/10^5 Pa \quad \ldots\ldots\ldots\ldots\ldots\ldots\ [15]$$

The point (2.90, 18.5) appears to depart significantly from the remaining three points which appear to fall on a straight line passing through the origin. If that point is dropped from the calculations a slope of b_S = 4.56 $\mu m/10^5 Pa$ is obtained. We thereby obtain an antagonism ratio of 1.6 if the questionable point is included and 1.5 if it is not. Furthermore, the pressure influence coefficients as well as the antagonism ratio for the *Vicia faba* studied by Glinka using the plasmolytic method appear to be very close to the corresponding values for *Tradescanta virginiana* studied by Edwards et al. using a direct method.

Edwards et al. also discuss the Spannungsphase (stress phase) which occurs before the pore opens. Physically this corresponds to the ventral walls of the guard cells being pressed tightly against each other. We claim that the Spannungsphase corresponds to those (P_g, P_S) combinations in Figs. 15 and 16 for which W < 0. Whenever P_g is sufficiently large or P_S sufficiently small, the W = 0 line is crossed and the pore opens. Consequently, when the influence coefficients are being determined, the pressure changes from the incipient opening state should be used, as was noted by Edwards et al. A dynamic analysis of stomatal behavior involving both stress phase and motor phase has recently been completed by Delwiche (1976).

DISCUSSION OF TABLE I

The influence coefficients of Table 1 characterize the bahavior of the shell for 14 different sets of parameters. For any P_g, P_S pressure combination, the eight displacement components shown in Fig. 6 may be obtained using equation [4]. Recall, however, that the influence coefficients for w_1 must be doubled to correspond to the influence

coefficients used in equation [6] to obtain the pore width W. The antagonism ratio, however, is the negative of the tabulated a_s/a_g ratio.

All parameters for the shell, except those mentioned in the table, were held constant for the 14 cases. Specifically, the initial configuration [A = 11 μm, B = 1.5 μm, C = 8 μm, D = 6 μm], two of the shell material properties [E_Θ = 500 $\mu N/(\mu m)^2$ and ν_Φ = 0.39], and the properties of the plate in the end of the shell [$E_\eta = E_\Phi$ = 2500 $\mu N/(\mu m)^2$, $\nu_\eta = \nu_\Phi$ = 0.39] were not varied. The positive directions for the 8 selected displacement components are shown in Fig. 6. Since each displacement component depends upon the combination of two pressures, the discussion will describe the response to P_g with P_s constant and then the response to P_s with P_g constant.

Set 2

Since an elliptical torus with a uniform wall thickness of 2 μm and a E_Φ/E_Θ ratio of 5 has many of the properties associated with stomata, including an antagonism ratio of 1.55, that case [Set 2 with E_Θ = 50 $\mu N/(\mu m)^2$, adjusted using equation [5]] was chosen for the figures and will be described in more detail here and will then be used as a basis for discussion of the remaining 13 sets.

With P_s held constant, P_g causes the shell to deform as follows: (1) the pore becomes wider; (2) the width of the cross section at $\Theta = 0$ decreases since node 265 moves towards node 1; (3) the height of the cross section increases by slightly more than w_1, (but by half the increase in pore width); (4) the horizontal motion at node 111, v_{111}, is approximately one-third the motion at node 1; (5) the pore length decreases slightly, i. e., approximately 4 percent of $2w_1$ and (6) the cross section at the elliptic plate is increased only very slightly in length and height.

Conversely, if P_g is held constant, P_s causes the shell to deform as follows: (1) the pore becomes narrower; (2) node 265 moves about the same distance and in the same direction as does node 1; (3) the height of the cross section at $\Theta = 0$ changes very little. Consequently, the response to P_s at $\Theta = 0$ is nearly rigid body motion towards the pore. It also follows that the horizontal motion at node 111 is nearly the same as the motion at node 1, (4) the subsidiary cell pressure has an insignificant effect on the motion of the elliptic plate and on the pore length.

Wall Thickness

Sets 1 and 7 and 3 and 8 differ only with respect to changes in the uniform wall thickness. The magnitudes of the influence coefficients for w_1 change significantly. For changes in P_g only, the reduction in thickness from 2.0 μm to 0.5 μm produces a 20-fold increase in displacement w_1. But for changes in P_s (with P_g constant), the w_1 displacement is virtually unchanged when E_Φ/E_Θ = 10 but actually reverses direction when E_Φ/E_Θ = 1.0. When the wall is isotropic and too thin, increasing P_s can actually cause the pore to open further! The thin walls also adversely affect the antagonism ratio. For set 7 the pressures actually reinforce, rather than oppose each other. For set 8 the antagonism ratio is much less than one. Such a system would probably not function satisfactorily. We may conclude that increasing either the thickness or the orthotropic ratio, E_Φ/E_Θ, causes the antagonism ratio to increase.

A variable wall thickness (Fig. 13) was used in sets 4, 5 and 6. Comparison with sets 1, 2 and 3, respectively, reveals very minimal change in sensitivity of pore width of P_g and P_s. The antagonism ratio is, therefore, unchanged. The most striking differences occur at nodes 111 and 265. The motion out of the plane is somewhat greater when the dorsal wall is thinner and deformation is primarily related to P_g. Likewise, the response of node 265 to P_g is increased. Unrealistically large deformations of the ventral guard cell wall towards the guard cell interior occur with the cross section of Fig. 13 unless E_Φ/E_Θ is greater than 10.

Micellae

For sets 1 through 6, in which E_Φ/E_Θ equals 1, 5 and 10, the antagonism ratio changes from 1.0 to 1.5 and to 1.9. On the basis of this trend, we believe that the micellae play a significant role in establishing the stomatal antagonism ratio. Without the micellae, a much thicker guard cell would be required for the stomate to function properly, unless, say, P_s were to be larger than P_g.

Elliptic Plate

Comparison of sets 1 and 11 (with E_Φ/E_Θ = 1) reveals that if the elliptic plate were absent, the out-of-plane motion at the plate ($\Theta = \pi/2$) would significantly increase in response to P_g.

Also, without the elliptic plate, the overall length of the stomatal apparatus *decreases* with increases in P_g, in contrast to sets 1 through 8. On the other hand, the pore length either increases (set 13) when P_g increases or decreases less than when a plate is present.

Constrained Pore Length

In sets 9, 10, and 14 the pore length and the shell cross section at $\Theta = \pi/2$ were constrained. Sets 1 and 9 and 3 and 10 may be compared directly. When E_Φ/E_Θ = 1, the principal difference appears to be that when the length is constrained, the pore length cannot shorten even slightly and, therefore, the pore opens slightly less (with $P_g = 6 \times 10^5$Pa, $P_s = 1 \times 10^5$ Pa) than for the unconstrained cases. For practical purposes, we can say that for the parameters and pressures considered, this constraint produced negligible changes.

SUMMARY

An elliptical torus model of kidney-shaped guard cells has been presented and analyzed using the finite element method. Computer-generated perspective figures have been presented to illustrate predicted deformations. Parameter sensitivity studies have been performed to explore the influence of guard cell and epidermal cell pressures, micellae, wall thickness, and guard cell geometry. This analysis has led to a theory for the interpretation of recent experiments conducted by Glinka and by Edwards, Meidner and Sheriff.

CONCLUSIONS

1 The elliptical shell model presented in this paper exhibits many of the qualitative responses known to exist in kidney-shaped stomates. The quantitative results are also reasonable but, of course, are based upon plausible estimates, rather than experimentally measured parameters.

2 The model predicts that the pore length remains relatively constant during opening and closing; this property need not be included *a priori* as an assumption.

3 The pore opening of the elliptical torus shell is a consequence of the decrease in guard cell cross section of the leaf and the concomitant deformation of the guard cell out of the plane

of the leaf.

4 Guard cell geometry plays an important role in stomatal behavior. For example, a standard, circular torus — a special case of the elliptical torus — does not respond properly to turgor pressure changes in the guard cell.

5 Stomatal opening and closing depends inherently upon the interaction, i. e., the opposition, of the guard cell and adjacent epidermal cell, as suggested by von Mohl as early as 1856.

6 In general, the pore width may be expressed as a multilinear function of the pressure in the guard cells and in the adjacent epidermal cells (equation [6]).

(a) The width cannot be described by the pressure difference alone.

(b) The partial regression coefficients in the multilinear relationship are the influence coefficients of the two pressures upon pore width. Consequently, these *influence coefficients* may be used to characterize the behavior of the stomate. The opposing roles of the guard cells and the adjacent subsidiary cells may be characterized by the explicitly defined *stomatal antagonism ratio* (equation [12]).

7 Although shell thickness variations do affect guard cell deformation, the presence of a "thin" dorsal wall and a "thick" ventral wall does not appear to mechanically enhance the structural aspects of stomatal opening.

8 A sufficiently thick elliptical torus model will open satisfactorily even in the absence of the radial stiffening by micellae. The structural importance of radial stiffening appears to be the increase produced in the stomatal antagonism ratio, a, i. e., the relative influence of the guard cell and "subsidiary" cell pressures upon pore width.

9 The experimental results of Glinka, who used a plasmolytic technique, and Edwards, Meidner and Sheriff, who used a direct pressure measurement technique, are reinterpreted and are shown to be in harmony with the theory presented in this paper.

10 The Spannungsphase (stress phase) behavior of stomates is shown to occur in an identifiable, triangular region of the P_gP_s plane.

11 Although Glinka's (1971) data (Fig. 15) supports the validity of the use of a linear thin shell theory, a nonlinear analysis would be a logical extension of this work.

APPENDIX A
INFLUENCE COEFFICIENTS

The P_g vs ψ and P_s vs ψ curves of Fig. 14 have slightly different slopes, so the pressure difference (P_g–P_s) varies slightly with ψ. The influence coefficient b_g may be computed in a manner which includes this slightly more general case.

Since

$$W = f_1(P_g, P_s) \quad \ldots\ldots\ldots\ldots \quad [A1]$$

where the pressures are given in parametric form by

$$P_g = f_2(\psi) \quad \ldots\ldots\ldots\ldots \quad [A2]$$

and

$$P_s = f_3(\psi), \quad \ldots\ldots\ldots\ldots \quad [A3]$$

the chain rule for the total derivative of the pore width with respect to the water potential, ψ, gives

$$\frac{dW}{d\psi} = \frac{\partial W}{\partial P_g}\bigg|_{P_s} \frac{dP_g}{d\psi} + \frac{\partial W}{\partial P_s}\bigg|_{P_g} \frac{dP_s}{d\psi} \quad \ldots\ldots\ldots\ldots \quad [A4]$$

From equation [A4] we obtain

$$b_s = \frac{\partial W}{\partial P_s}\bigg|_{P_g} = \left[\frac{dW}{d\psi} - \frac{\partial W}{\partial P_g}\bigg|_{P_s} \frac{dP_g}{d\psi}\right] \Big/ \left[\frac{dP_s}{d\psi}\right] \quad \ldots\ldots\ldots\ldots \quad [A5]$$

From Fig. 14 we obtain

$$dW/d\psi = [14.4 - 6.7] \,/\, [(-6) - (0)] = -1.28 \quad \ldots\ldots\ldots\ldots \quad [A6]$$

$$\partial W/\partial P_g\Big|_{P_s} = b_g = [4.4 - 13.1]/[2 - 5] = 2.90\ \mu m/(10^5 Pa) \quad \ldots\ldots\ldots\ldots \quad [A7]$$

$$dP_g/d\psi = [6.0 - 12.0]/[(-6) - (0)] = 1.00 \quad \ldots\ldots\ldots\ldots \quad [A8]$$

$$dP_s/d\psi = [0.9 - 6.5]/[(-6) - (0)] = 0.93 \quad \ldots\ldots\ldots\ldots \quad [A9]$$

Using these values in (A5) gives

$$b_s = -4.48\ \mu m/(10^5 Pa) \quad \ldots\ldots\ldots \quad [A10]$$

The stomatal antagonism ratio becomes

$$a = -b_s/b_g = 4.48/2.90 = 1.54 \quad \ldots\ldots [A11]$$

APPENDIX B
CIRCULAR TORUS

Consider an elastic circular torus (A = B, C = D) loaded under uniform internal pressure ($P_g = P$, $P_s = 0$).

In order to determine whether the shell opens or closes under this load (i. e., upon inflation), it is sufficient to know the sign of the resulting normal displacement W at the inner circular boundary, $\Phi = -\pi/2$. (Positive W means the shell opens upon inflation.)

The linear strain ϵ_Θ at $\Phi = -\pi/2$ due to W is (Fig. 5)

$$\epsilon_\Theta = \frac{\Delta L}{L} = \frac{2\pi(B+W) - 2\pi B}{2\pi B} = \frac{W}{B} \quad \ldots [B1]$$

Hooke's Law for an orthotropic shell gives (Lekhnitskii (1968), p. 46).

$$\epsilon_\Theta = \frac{N_\Theta - \nu_\Theta N_\phi}{E_\Theta h} \quad \ldots\ldots\ldots\ldots \quad [B2]$$

where

h = uniform shell thickness
N_Θ, N_Φ = shell membrane force per unit length
$E_\Theta\ \eta_\Phi$ = $E_\Phi\ \nu_\Theta$ (Lekhnitskii 1968, p. 46).

The linear membrane theory of shells applied to the circular torus gives at $\Phi = -\pi/2$ (see, e.g., Novozhilov 1959, p. 305).

$$N_\Theta = \frac{pC}{2},\ N_\phi = \frac{pC}{2B}(2B + C) \quad \ldots\ldots [B3]$$

From equations [B1] — [B3], find

TABLE 2. CIRCULAR TORUS.

Parameters: Thickness $2\mu m$; $E_\Theta = 500\ \mu n/(\mu m)^2$; B = $1.5\mu m$; C = $8\mu m$

SET	1A		2A		3A	
E_ϕ/E_Θ	1.0		5.0		10.0	
	a_g	a_s	a_g	a_s	a_g	a_s
W_1	-0.010	0.0002	0.0014	0.0030	0.0034	0.0025
membrane W_1	(-0.011)		(0.0026)		(0.0043)	
V_{111}	0.028	-0.041	-0.034	-0.049	0.033	-0.047
W_{111}	-0.129	-0.057	-0.0065	-0.051	0.0048	-0.041
W_{265}	-0.014	0.101	-0.048	0.098	-0.047	0.085
α	0.02		-2.2		-0.74	

$$W = \frac{pC}{2E_\Theta h}\,[B - \nu_\Theta\,(2B + C)] \quad \ldots \quad [B4]$$

Therefore the shell opens upon inflation (W>0) if and only if (iff)

$$\frac{B}{C} > \frac{\nu_\Theta}{1-2\nu_\Theta} \quad \ldots\ldots\ldots\ldots\ldots \quad [B5]$$

If we assume $\nu\Phi = 0.39$ then $\nu\Theta = \nu\Phi/(E\Phi/E\Theta)$ and $\nu\Theta$ depends on both $\nu\Phi$ and $E\Phi/E\Theta$. In particular for isotropy ($E\Phi/E\Theta = 1$), the shell opens iff $B/C > 1.77$. For an orthotropic material with $E\Phi/E\Theta = 5$, however, the shell opens iff $B/C > 0.092$.

It is to be noted that although it has been shown in the literature (Dean 1939) that bending stresses are important near $\Phi = 0, \pi$, this computation, based upon the linear membrane theory of shells, is concerned only with $\Phi = \pi/2$, where bending stresses are small.

The above membrane analysis shows qualitative agreement with a more general finite element shell analysis which also includes bending stresses. A 24 element, 89 node mesh was used. The node numbering in Table 2 has been altered to agree with Table I and Fig. 6. The three conditions correspond to sets 1, 2 and 3 of Table I with the pore length reduced to the pore width (A = B) and with the cross-section made circular by increasing the height (D = C).

An isotropic, circular torus model will not function properly as a stomate since the pore actually becomes smaller when P_g is increased with P_s held constant since $a_g = -0.010$ in Set 1A. If orthotropic properties are now introduced (sets 2A and 3A) the appropriate sign on a_g is obtained but the sign on a_s does not reverse. In other words, for constant P_g, an increase in P_s on the outer perimeter of the torus actually causes the pore to open further. Furthermore, in all three cases the antagonism ration is unrealistic.

References

1 Ashwell, D. G. and R. H. Gallagher (eds.). 1976. Finite elements for thin shells and curved members. John Wiley & Sons, London.

2 Aylor, Donald E., Jean-Yves Parlange, and A. D. Krikorian. 1973. Stomatal mechanics. Amer. J. Bot. 60(2):163-171.

3 Aylor, Donald E., Jean-Yves Parlange, and Abraham D. Krikorian. 1975. Comment on some recent models of stomatal mechanics. J. Theor. Bio. 54, 395-397.

4 Bidwell, R. G. 1974. Plant physiology. MacMillan, NY, p. 298.

5 Bushnell, D. 1974. Thin shells in structural mechanics computer programs: surveys, assessments, and availability. W. Pilkey et al., Editors. University of Virginia Press. Charlottesville, VA.

6 Cook, Robert D. 1974. Concepts and applications of finite element analysis. John Wiley and Sons, Inc., New York.

7 Dawe, D. J. 1971. Curved finite elements in the analysis of shell structures. Proc. First SMIRT, Vol. 4, Part J, Paper J 1/4, Berlin.

8 Dean, W. R. 1939. Distortion of a curved tube due to internal pressure. Phil. Mag., Ser. 7(28):452.

9 Delwiche, M. J. 1976. An analytical model of the hydraulic aspects of stomatal dynamics. MS Thesis. Department of Agricultural Engineering. Cornell University, Ithaca. 172 p.

10 DeMichele, Don W. and Peter J. H. Sharpe. 1971. A model of stomatal action: its agronomic and ecological significance. ASAE Paper 71-589, St. Joseph, MI 49085. (Microfiche) 40 p.

11 DeMichele, Don W. and Peter J. H. Sharpe. 1973. An analysis of the mechanics of guard cell motion. J. Theor. Biol. 41:77-96.

12 DeMichele, Don W. and Peter J. H. Sharpe. 1974. A parametric analysis of the anatomy and physiology of the stomata. Agricultural Meteorology 14:229-241.

13 Edwards, Mary, Hans Meidner and D. W. Sheriff. 1976. Direct measurements of turgor pressure potentials of guard cells. II. The mechanical advantage of subsidiary cells, The Spannungsphase, and the optimum leaf water deficit. Journal of Experimental Botany 27(96): 163-171.

14 Esau, K. 1965. Plant Anatomy. 2nd ed. John Wiley and Sons, NY.

15 Forsberg, K. and R. Hartung. 1971. An evaluation of finite difference and finite element techniques for general shells. Proc. IUTAM Symp. on High Speed Comp. of Elastic Structures, B. Fraeijs de Veubeke, Ed., 2:837-859.

16 Gallagher, R. H. 1969. Analysis of plate and shell structures. Proc. of Conf. on Application of Finite Element Methods in Civil Engrg. Vanderbilt University. pp. 155-206.

17 Gallagher, R. H. 1975. Finite element analysis: fundamentals. Prentice Hall. Englewood Cliffs, NJ.

18 Gallagher, R. H. 1975. Shell Elements. World Conference on F.E.M., Bournemouth, England.

19 Glinka, Z. 1971. The effect of epidermal cell water potential on stomatal response to illumination of leaf discs of **Vicia faba.** Physiologia Plantarum 24:476-479.

20 Guttenberg, Hermann von. 1959. Die physiologische Anatomie der Spaltöffnungen. p. 399-414. In W. Ruhland (ed.) Handbuch der Pfanzenphysiologie. Band 17. Springer Verlag, Berlin-Göttingen-Heidelberg.

21 Heath, O.V.S. 1959a. The water relations of stomatal cells and the mechanisms of stomatal movement. p. 193-250. In F. C. Steward (ed.) Plant Physiology, A Treatise. Vol. 2.

22 Heath, O.V.S. 1959b. Light and carbon dioxide in stomatal movements. In W. Ruhland, ed. Handbuch der Pflanzenphysiologie 17(2), Springer, Berlin.

23 Huber, M. T. 1925. Über die genaue Berechnung einer orthotropen Platte, der Bauingenieur, Berlin. 6(30):878-879.

24 Huebner, Kenneth. 1975. The finite element method for engineers. John Wiley and Sons, NY.

25 Kanodia, V. L. 1976. Finite element elastic instability analysis of deep shells of double curvature. Ph.D. Dissertation, Cornell University, Ithaca, NY.

26 Kramer, Paul J. 1959. Transpiration and the water economy of plants. In F. C. Steward (ed.) Plant physiology. Vol. 2. Academic Press. New York.

27 Lekhnitskii, S. Q. 1968. Anisotropic plates, translated from the second Russian edition by S. W. Tsai and T. Cheron, Gordon and Breach Science Publishers, New York, London, Paris. pp. 45-50, 273-282.

28 Mang, H. A. and R. H. Gallagher. 1976. A critical assessment of the simplified hybrid displacement method. Accepted for publication in the International Journal of Numerical Methods in Engineering.

29 Mang, H. A., R. H. Gallagher and V. L. Kanodia. 1976. Finite element shell instability (FESIA) Report. Department of Structural Engineering. Cornell University, Ithaca, New York.

30 Meidner, Hans and Mary Edwards. 1975. Direct measurements of turgor pressure potentials of guard cells, I. Journal of Experimental Botany 26(92):319-330.

31 Meidner, Hans and T. A. Mansfield. 1968. Physiology of stomata. McGraw-Hill, New York.

32 Meyer, Bernard S., Donald B. Anderson, Richard H. Böhning. 1969. Introduction to plant physiology. D. Van Nostrand, N.Y., p. 84.

33 Mohl, H. von. 1856. Welche Ursachen bewirken die Erweiterung und Verengung der Spaltöffnungen. Botanische Zeitung 14:697-704; 713-721.

34 Moon, P. and D. E. Spencer. 1961. Field theory for engineers. D. Van Nostrand, Company Inc., Princeton, New Jersey. p. 204.

35 Nobel, P. S. 1974. Introduction to biophysical plant physiology. W. H. Freeman & Co., San Francisco.

36 Novozhilov, V. V. 1959. The theory of thin shells. Noordhoff, Netherlands.

37 Raschke, K. 1975. Stomatal action. In Ann. Rev. Plant Physiology. 26:309-40.

38 Schwendener, S. 1881. Über Bau und Mechanik der Spaltöffnungen. Monatsberichte der Berliner Akademie der Wissenschaften 46: 833-867, in Schwendener, S. 1898. Gesammelte Botanische Mittheilungen. 33-70. Verlag von Gebrüder Borntraeger, Berlin.

39 Segerlind, L. J. 1976. Applied finite elements. John Wiley and Sons. New York.

40 Shoemaker, E. M. and L. M. Srivastava. 1973. The mechanics of stomatal opening in corn (Zea mays L.) leaves. J. Theo. Biol. 42:219-225.

41 Slatyer, R. O. 1967. Plant-water relationships. Academic Press, NY.

42 Snedecor, George W. and William G. Cochran. 1967. Statistical methods, 6th edition, Chapter 13. The Iowa State University Press, Ames, Iowa.

43 Stålfelt, M. G. 1966. The role of the epidermal cells in the stomatal movements. Physiologia Plantarum. 19:241-256.

44 Thomas, G. R. 1973. Finite element nonlinear analysis of shells. Ph.D. Dissertation, Cornell University. Ithaca, NY.

45 Thomas, G. R. and R. H. Gallagher. 1976. A triangular element based on generalized potential energy concepts in finite elements for thin shells and curvey members. Ashwell and Gallagher (eds.) John Wiley & Sons, London, pp. 155-169.

46 Thomas, G. R. and R. H. Gallagher. 1975. A triangular thin shell finite element: linear analysis. NASA Report CR-2482. 41 pgs.

47 Thomas, G. . and R. H. Gallagher. 1975. A triangular thin shell finite element: nonlinear analysis. NASA Report CR-2483. 64 pgs.

48 Troughton, John and Lesley A. Donaldson. 1972. Probing plant structure. Chapman and Hall, London.

49 Ursprung, A. and G. Blum. 1924. Eine Methode zur Messung des Want-Turgordruckes der Zelle, nebst Anwendungen. Jahrbücher für Wissenschaftliche Botanik 63. 1-110. Fitting, H. (ed.) Verlag von Gebrüder Borntraeger, Berlin.